

S-allylCysteine Ester/Caffeic Acid Amide Hybrids as Promising Antiprotozoal Candidates: Synthesis, Biological Evaluation and Molecular Modeling Studies

Wilson Cardona-G¹, Sara Maria Robledo²,
Laura Juliana Prieto¹, Andrés Felipe Yépes^{1*}

¹Química de Plantas Colombianas, Institute of Chemistry, Faculty of Exact and Natural Sciences, Universidad de Antioquia, Medellín, Colombia, ²PECET-Medical Research Institute, School of Medicine, Universidad de Antioquia, Medellín, Colombia

In order to overcome the challenges of discovering new antiprotozoal drugs, we synthesized a new class of hybrids based on S-allylCysteine Ester/Caffeic Acid Amide and evaluated four of them against *Trypanosoma cruzi* and *Plasmodium falciparum*. Hybrid **6** exhibited good activity on *T. cruzi* with an EC₅₀ value of 5.45 μM, whereas hybrid **3** was active over *P. falciparum* with an EC₅₀ of 18.08 μM. All hybrids displayed a good selectivity index on *P. falciparum*. Molecular docking computations indicated that several hybrids have good binding affinities towards the protozoa related enzymes (Cruzipain or Falcipain-2) when compared against current inhibitors. *In silico* studies showed that conjugates **1-3** and **6** fulfilled optimal ADME characteristics, suggesting them as safe alternatives for oral treatment of protozoal infections.

Keywords: S-allyl cysteine. Caffeic acid. Hybrid. Chagas disease. Malaria disease. Modelling studies.

INTRODUCTION

Protozoal infections are a diverse group of diseases which are the cause of significant morbidity and mortality in numerous developing countries of tropical and subtropical regions. Parasitic diseases include, among others, malaria and Chagas disease (American trypanosomiasis), which are caused by the parasitic protozoan of *Plasmodium* and *Trypanosoma cruzi*, respectively (WHO, 2018a). Human malaria is caused by at least five species of *Plasmodium*, the most important being *P. falciparum* and *P. vivax* (WHO, 2018b).

The drugs used for chemotherapy against these diseases are nitroaromatic compounds (benznidazole and nifurtimox) for the treatment of Chagas disease (WHO, 2019) and chloroquine, amodiaquine, sulfadoxine/

pyrimethamine, and Tafenoquine to treat *P. falciparum* or *P. vivax* malaria, respectively (Figure 1). More recently a new artemisinin-based combination therapy was recommended for the treatment of *P. falciparum* (WHO, 2018b). Unfortunately, all of these drugs have several toxic effects on the patients that are associated with high doses and long therapeutic schemes. Moreover, they are no longer as effective as before due to the emergence of drug resistance in the parasite, which complicates the control of these diseases (Keenan, Chaplin, 2015; Chatelain, Ioset, 2011; Fidock *et al.*, 2004).

*Correspondence: A. F. Yepes. Química de Plantas Colombianas. Faculty of Exact and Natural Sciences. Institute of Chemistry. Universidad de Antioquia, 57 (4) 219 5650, Medellín, Colombia. E-mail: andresf.yepes@udea.edu.co. ORCID: <https://orcid.org/0000-0001-6975-5119>

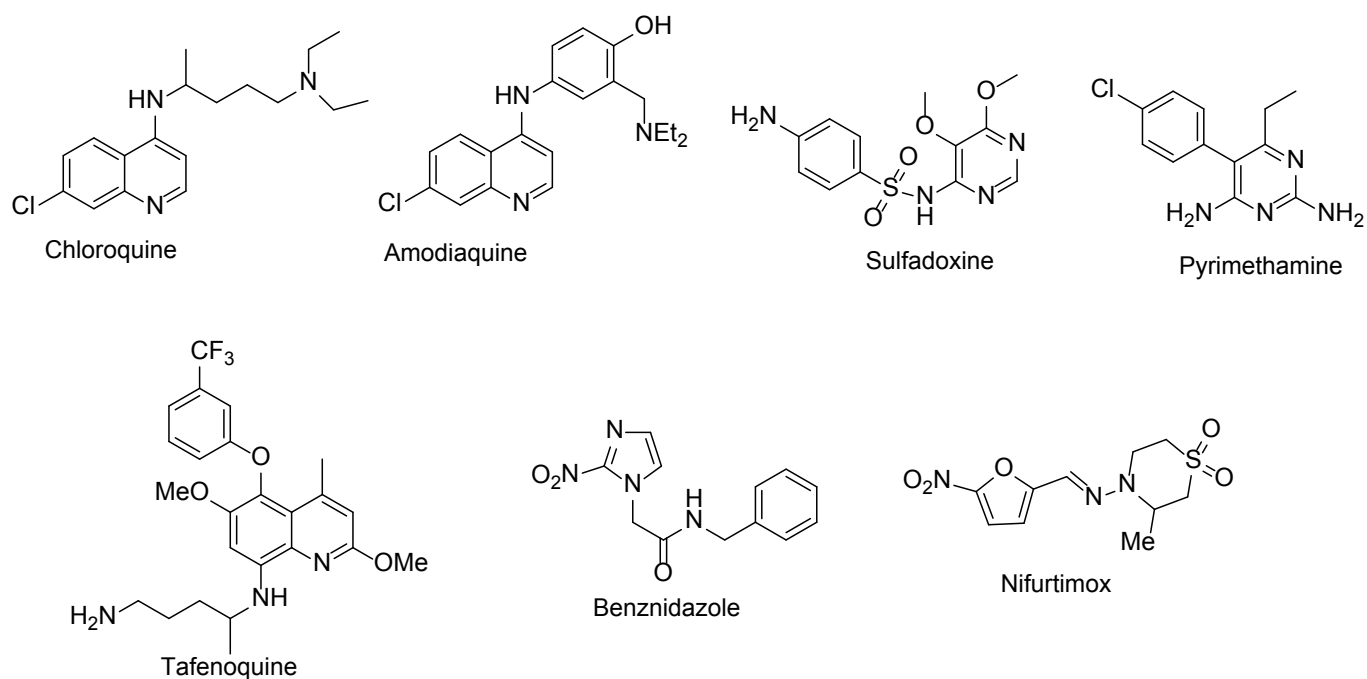


FIGURE 1 - FDA-approved antiparasitic drugs available to treat Chagas and malaria diseases.

Garlic (*Allium sativum* L.) has acquired a reputation in different traditions as a prophylactic as well as a therapeutic medicinal plant. Medicinal benefits and therapeutic properties of garlic are ascribed to the presence of organosulfur compounds, among these, allylcysteine (**A**) (Figure 2) (Foroutan-Rad, Hazrati, Khademvatan, 2017). Several studies have shown that the extract of garlic was effective against a host of protozoa including rodent *Plasmodium* (*P. berghei* and *P. yoelii*) (Coppi *et al.*, 2006) and African *Trypanosoma* species (*T. brucei brucei*, *T. congolense*, and *T. vivax*) (Nok, Williams, Onyenekwe, 1996).

Caffeic acid (**B**) and its derivatives (Figure 2) display a broad spectrum of biological properties (Otero *et al.*, 2014; De *et al.*, 2012; Hung *et al.*, 2005;

Son, Lewis, 2002; Rajan *et al.*, 2001), antitrypanosomal and antiplasmodial activities among them. On one hand, Caffeic acid exhibited high activity and selectivity index against *T. b. rhodesiense* with an IC_{50} of 6.10 μ M and SI of 48.5 (Tasdemir *et al.*, 2006). This compound cured five out of five mice infected with *T. b. brucei* EATRO 110 (Shapiro *et al.*, 1982) after an i.v. dose of 100 mg/kg. On the other hand, in an *in-vitro* assay based on plasmodial lactate dehydrogenase activity, caffeic acid ethyl ester (**C**) exhibited an IC_{50} of 21.9 ± 9.4 μ M. This compound showed an *in vivo* growth inhibition of 55% at 100 mg/kg (Alson *et al.*, 2018). **D** was the most active compound against *T. cruzi* among a series of caffeic acid-triclosan hybrids, with an IC_{50} of 8.25 μ M, showing higher activity than benznidazole ($IC_{50} = 40.3$ μ M) (Otero *et al.*, 2017).

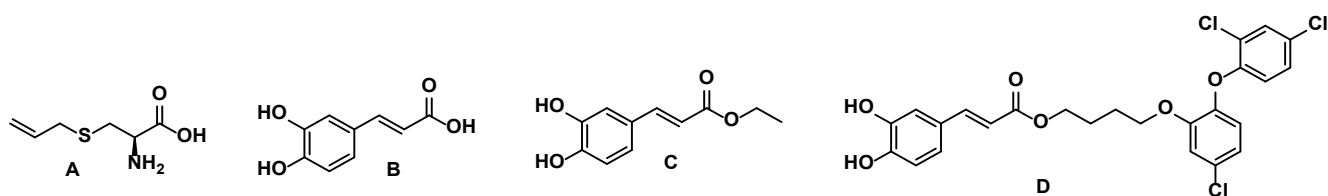


FIGURE 2 - Chemical structures of allylcysteine, caffeic acid and caffeic acid derivatives.

Enzymes represent very attractive targets for new small molecule drugs for therapeutic intervention in human parasitic diseases (Siles *et al.*, 2006; Fujii *et al.*, 2005). In this scenario, cruzipain and falcipain-2 (FP-2), are the most important cysteine proteases that display many important activities against *T. cruzi* and *P. falciparum*, respectively, such as invasion in the host cells, nutrition, and differentiation of the parasite besides interference in the host immunological system mechanisms (Duschak *et al.*, 2001; McGrath *et al.*, 1995). All of the above make these enzymes a useful molecular target to design anti-trypanosomal agents, particularly by using computational methods for mapping out the mechanism of action of promising anti-parasitic drug candidates. (Vieira, Santos, Ferreira, 2019; McKerrow *et al.*, 2006). Several studies have shown that the presence of an α,β -unsaturated carbonyl group confers the necessary reactivity to inhibit cysteine-proteases, specially cruzipain and falcipain-2. The data regarding α,β -unsaturated compounds showed

strong in vitro inhibitory potency against cruzipain from *T. cruzi* and FP-2 from *P. falciparum*, making them highly efficient in blocking the enzymatic activity in protozoan systems (Machin, Kantsadi, Vakonakis, 2019; Tiwari *et al.*, 2017; Borchhardt *et al.*, 2010; Yang *et al.*, 2009; Santos, Moreira, 2007; Kunakbaeva, Carrasco, Rozas, 2003; Hans-Hartwig, Tanja, 1997).

There is an emerging strategy in medicinal chemistry and drug discovery research based on obtaining hybrid molecules that combine two or more structural fragments of drugs that have a relevant pharmacological action (Ivasiv *et al.*, 2019; Gupta *et al.*, 2010; Provencher-Mandeville *et al.*, 2008; Viegas-Junior *et al.*, 2007). These hybrids may display dual activity but do not necessarily act on the same biological target (Meunier, 2008; Tsogoeva, 2010). Based on the above, we decided to evaluate the antiprotozoal activity and *in silico* properties of several S-allyl cysteine ester–caffeic acid amide hybrids (Figure 3).

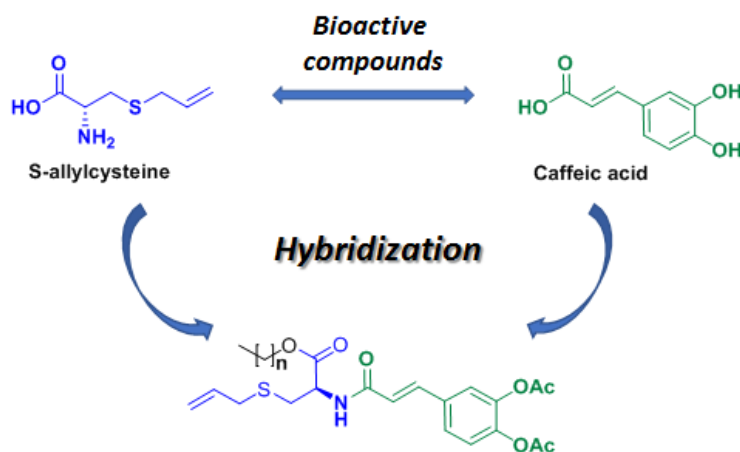


FIGURE 3 - Design of S-allyl cysteine-ester-caffeic acid amide hybrids as antiprotozoal agents.

MATERIAL AND METHODS

Chemical synthesis

General remarks

^1H and ^{13}C NMR spectra were recorded on a Varian instrument operating at 300 and 75 MHz, respectively. The signals of the deuterated solvent (CDCl_3) were

used as reference. Chemical shifts (δ) are expressed in ppm with the solvent peak as reference and TMS as an internal standard; coupling constants (J) are given in Hertz (Hz). Carbon atom types (C, CH, CH_2 , CH_3) were determined using the DEPT pulse sequence. Signals were assigned using two-dimensional homonuclear (COSY) and heteronuclear (HSQC and HMBC) correlations. High resolution mass spectra were recorded using electrospray ionization mass spectrometry (ESI-MS). A QTOF Premier

instrument with an orthogonal Z-spray-electrospray interface (Waters, Manchester, UK) was used operating in the W-mode. The drying and cone gas was nitrogen, set to flow rates of 300 and 30 L/h, respectively. Methanol sample solutions (ca. 1×10^{-5} M) were directly introduced into the ESI spectrometer at a flow rate of 10 μ L/min. A capillary voltage of 3.5 kV was used in the positive scan mode, and the cone voltage was set to $U_c = 10$ V. For accurate mass measurements, a 2 mg/L standard solution of leucine enkephalin was introduced via the lock spray needle at a cone voltage set to 85 V and a flow rate of 30 μ L/min. IR spectra were recorded on a Spectrum RX I FT-IR system (Perkin-Elmer, Waltham, MA, USA) in KBr pellets. Optical rotations were measured (Na-D line) at 25°C using a cell with 1 dm path length on a Polartronic (Jasco model p-2000) polarimeter. Silica gel 60 (0.063–0.200 mesh, Merck, Whitehouse Station, NJ, USA) was used for column chromatography, and precoated silica gel plates (Merck 60 F254 0.2 mm) were used for thin layer chromatography (TLC). Monitoring of the reaction progress and product purification was carried out by TLC.

Synthesis of Octyl S-prop-2-en-1-ylcysteinate (4): Thionyl chloride (3eq) was added over 5 min. to dry octyl alcohol (15 mL) cooled to -10°C and the resulting solution stored for an additional 5 min. Then, S-allyl cysteine (500 mg, 3.1 mmol) was added and the resulting mixture was stored at -10°C for 2h and then kept at room temperature for additional 24h. Then the excess of alcohol was removed by distillation under reduced pressure. The residue was purified by column chromatography over silica gel eluting with dichloromethane-methanol (95:5 ratio) to obtain S-allyl cysteine octyl ester in 50% yield. Monitoring of the reaction progress and product purification was carried out by TLC. $[\alpha]^{25} + 2.238$ (C = 0,019, CHCl_3); IR (KBr, cm^{-1}): ν_{max} 3393 (N-H), 1735 (C=O), 1265 (C-O-C); $^1\text{H NMR}$ (CDCl_3 , 300 MHz): δ 0.90 (3H, t, $J = 6.9$ Hz), 1.24-1.45 (8H, m), 1.62-1.74 (4H, m), 1.81 (NH_2), 2.72 (1H, dd, $J = 13.5, 7.3$ Hz, S- CH_2CHN), 2.91 (1H, dd, $J = 13.5, 4.8$ Hz, S- CH_2CHN), 3.19 (2H, d, $J = 7.1$ Hz, S- $\text{CH}_2\text{CH}=\text{CH}_2$), 3.65 (1H, dd, $J = 7.6, 4.7$ Hz, -CH-N), 4.16 (2H, t, $J = 6.8$ Hz, OCH_2), 5.12-5.21 (2H,

m, S- $\text{CH}_2\text{CH}=\text{CH}_2$), 5.74-5.90 (1H, m, S- $\text{CH}_2\text{CH}=\text{CH}_2$); $^{13}\text{C NMR}$ (CDCl_3 , 75 MHz): δ 14.10 (CH_3), 22.64 (CH_2), 25.88 (CH_2), 28.55 (CH_2), 29.17 (2 CH_2), 31.79 (CH_2), 35.14 (S- CH_2CHN), 35.81 (S- $\text{CH}_2\text{CH}=\text{CH}_2$), 54.10 (CH-N), 65.42 (OCH_2), 117.53 (S- $\text{CH}_2\text{CH}=\text{CH}_2$), 134.0 (S- $\text{CH}_2\text{CH}=\text{CH}_2$), 174.19 (-C=O); EIMS: m/z 274.1841 $[\text{M} + \text{H}]^+$, Calcd for $\text{C}_{11}\text{H}_{22}\text{NO}_2\text{S}$: 274.1838.

Synthesis of Octyl N-{(2E)-3-[3,4-bis(acetyloxy)phenyl]prop-2-enoyl}-S-prop-2-en-1-ylcysteinate (6): A solution of 3,4-diacetoxycaffeic acid (5) (1 mmol) and triethylamine (4 mmol) in THF (10 mL) was stirred for 15 min. HBTU (1.5 mmol) was added and the resulting mixture was stirred for 10 min. Then, S-allyl cysteine ester (1.2 mmol) was added and the resulting mixture was allowed to stir for 15h. The solvent was removed under reduced pressure, and the residue was chromatographed on silica gel. Elution with hexane-ethyl acetate (1:1 ratio) afforded compounds 6 in 40%. $[\alpha]^{25} + 1.620$ (C = 0,0043, CHCl_3); IR (KBr, cm^{-1}): ν_{max} 3438 (N-H), 1776, 1740 and 1663 (C=O), 1203 (C-O-C), 1184 ((C=O)-O); $^1\text{H NMR}$ (CDCl_3 , 300 MHz): δ 0.93 (3H, t, $J = 6.9$ Hz), 1.24-1.47 (8H, m), 1.63-1.77 (4H, m), 2.35 (3H, s, ((CH_3 -C=O)-O), 2.36 (3H, s, ((CH_3 -C=O)-O), 2.92 (1H, dd, $J = 13.9, 5.3$ Hz, S- CH_2CHN), 3.1 (1H, dd, $J = 13.9, 4.8$ Hz, S- CH_2CHN), 3.18 (2H, d, $J = 7.25$ Hz, S- $\text{CH}_2\text{CH}=\text{CH}_2$), 4.21 (2H, t, $J = 6.9$ Hz, OCH_2), 4.79-4.89 (1H, m, -CH-N), 5.12-5.22(2H, m, S- $\text{CH}_2\text{CH}=\text{CH}_2$), 5.70-5.88 (1H, m, S- $\text{CH}_2\text{CH}=\text{CH}_2$), 6.46 (1H, d, $J = 15.6$ Hz, -CO-CH=), 7.26 (1H, d, $J = 8.3$ Hz, Ar-H), 7.40 (1H, d, $J = 1.6$ Hz, Ar-H), 7.44 (1H, dd, $J = 8.3, 1.6$ Hz, Ar-H), 7.64 (1H, d, $J = 15.6$ Hz, Ar-CH=C); $^{13}\text{C NMR}$ (CDCl_3 , 75 MHz): δ 14.12 (CH_3), 20.67 ((CH_3 -C=O)-O), 20.70 ((CH_3 -C=O)-O), 22.26 (CH_2), 23.22 (CH_2), 25.85 (2 CH_2), 28.51 (CH_2), 29.17 (CH_2), 29.18 (CH_2), 31.76 (CH_2), 32.89 (S- CH_2CHN), 35.27 (S- $\text{CH}_2\text{CH}=\text{CH}_2$), 52.09 (CH-N), 66.16 (OCH_2), 117.92 (S- $\text{CH}_2\text{CH}=\text{CH}_2$), 118.03 (=C-CO-), 121.05 (Ar), 122.52 (Ar), 123.9 (Ar), 126.33 (Ar), 133.57 (S- $\text{CH}_2\text{CH}=\text{CH}_2$), 140.23 (Ar-C=), 142.41 (Ar-O), 143.20 (Ar-O), 164.93 (N-C=O), 168.10 ((CH_3 -C=O)-O), 168.14 ((CH_3 -C=O)-O), 170.90 ((NCH-C=O)-O); EIMS: m/z 542.21884 $[\text{M} + \text{Na}]^+$, Calcd for $\text{C}_{27}\text{H}_{37}\text{NO}_7\text{S-Na}$: 542.2189

Biological activity assays

In vitro Cytotoxicity

Human promonocytic U-937 cells (ATCC CRL-1593.2TM) were grown in tissue flasks for five days and then harvested and washed with phosphate buffered saline (PBS) by centrifugation. Cells were counted and adjusted at 1×10^6 cells/mL of complete culture medium (RPMI-1640) supplemented with 10% Fetal Bovine Serum-FBS and 1% of antibiotics -100 U/mL penicillin and 0.1 mg/mL streptomycin. One hundred μ L of cell suspension were dispensed into each one of a 96-well cell-culture plate and then 100 μ L of two-fold serial dilutions of the compounds (starting at 200 μ g/mL) in complete RPMI 1640 medium were added. All plates were incubated at 37°C, 5% CO₂ during 72h. Then, 10 μ L/well of MTT solution (0.5 mg/mL) were added into each well, and all plates were then incubated at 37°C for 3h. Formazan crystals were dissolved by adding 100 μ L/well of dimethyl sulfoxide and 30 min incubation. Cell viability was determined according to the intensity of color (absorbance) registered as optical densities (O.D) obtained at 570 nm in a Varioskan™ Flash Multimode Reader-Thermo Scientific, USA spectrophotometer. Cells cultured in absence of compounds were used as control of viability (negative control), while doxorubicin was used as control for cytotoxic drugs. Non-specific absorbance was corrected by subtracting the O.D of the blank. Assays were conducted in two independent runs with three replicas per each concentration tested (Coa *et al.*, 2020).

In vitro antitrypanosomal Activity

T. cruzi, *Tulahuen* strains transfected with the β -galactosidase gene (donated by Prof. F. S. Buckner, University of Washington) were maintained *in vitro* as epimastigotes by culturing in modified Novy-McNeal-Nicolle (NNN) medium. The U-937 cells were adjusted at 2.5×10^6 cells/mL of complete RPMI-1640 medium containing 0.1 μ g/mL of phorbol myristate acetate to induce differentiation to macrophages. Then, 100 μ L of this cell suspension were dispensed into each one of a 96-

well cell-culture plate. After 24h of incubation at 37°C, 5% CO₂, macrophages were infected with early stationary growth phase (10 days in culture) epimastigotes, at the concentration of 12.5×10^5 parasites/mL of complete RPMI 1640 medium equivalent to 5:1 (parasites per cell) ratio. Plates were incubated at 34°C, 5% CO₂ for 24 hours to allow the conversion to intracellular amastigotes. Extracellular parasites were removed by washing twice with 100 μ L of PBS. Then, infected cells were exposed to 100 μ L of each compound at a concentration of 20 μ g/mL and plates were incubated at 34°C, 5% CO₂. After 72 h of incubation plate wells were washed twice with PBS and β -galactosidase activity was measured by spectrophotometry adding 100 μ M of the chromogenic substrate CPRG (chlorophenol red-beta-D-galactopyranoside) and 0.1% nonidet P-40 to each well. After 3h of incubation at 25 °C, absorbance was read at 570 nm in a Varioskan™ Flash Multimode Reader - Thermo Scientific, USA spectrophotometer. Infected cells exposed to benznidazole were used as control for antitrypanosomal activity (positive control) while infected cells incubated in complete RPMI 1640 culture medium were used as control for infection (negative control). Non-specific absorbance was corrected by subtracting the O.D of the blank. Determinations were done by triplicate in at least two independent experiments (García *et al.*, 2019). Those compounds that were able to reduce the number of intracellular parasites by more than 50% were tested again using four different concentrations (100 – 25 – 6.12 and 1.56 μ g/mL) of each compound.

In vitro Antiplasmodial Activity

Antiplasmodial activity was evaluated in asynchronous cultures of *P. falciparum* (NF54 strain), maintained in standard culture conditions. The effect of each compound over the growth of the parasites was determined by Plasmodium lactate dehydrogenase assay (pLDH) (Nkhoma, Molyneux, Ward, 2017; Londoño *et al.*, 2016). Parasites were plated in the trophozoite phase at 1% hematocrit and 0.5 % parasitemia in 100 μ L of each compound at specific concentrations (1000 – 25 – 6.25 – 1.56 μ g/mL). Plates were incubated in an atmosphere with a gas mixture of 4% O₂, 3% CO₂, and

97% N₂, and incubated at 37°C for 72 hours. Meanwhile, two reagents for detecting and measuring the LDH enzyme were prepared. The first of these was Malstat reagent (400 µL of Triton X-100 in 80 mL of deionized water, 4.0 g L-lactate, 1.32 g Tris buffer and 0.022 g of 3-acetylpyridine adenine dinucleotide (APAD), adjusting the pH to 9 with hydrochloric acid, and a volume of 200 mL with deionized water. The second reagent was a NBT/PES solution (1-6 g nitro blue tetrazolium salt and 0.008 g phenazine ethosulfate in 100 mL of deionized water. The solution was stored in a foil-covered container and kept at 4°C until required. When incubation was complete, plates were harvested and subjected to three 20-minute freeze–thaw cycles to resuspend the culture. Subsequently, 100 µL of Malstat reagent and 25 µL of NBT/PES solution were added to each well of a new, duplicate flat-bottomed 96-well cell culture plate. The culture in each of the wells of the original plate was resuspended by mixing with a multichannel pipette. Then, 15 µL of the culture were taken from each well and added to the corresponding well of the Malstat plate, thus initiating the LDH reaction. Color development of the LDH plate was monitored colorimetrically at 650 nm in the Varioskan Flash reader after one hour of incubation in the dark.

Data Analysis

Cytotoxicity was determined according to cell growth (viability) and mortality percentages obtained for each isolated experiment (compounds, doxorubicin and culture medium). Percentage of viability was calculated by Equation 1, where the optical density (O.D) of control corresponds to 100 % of viability (cell growth).

$$\% \text{ Mortality} = 1 - \left[\frac{(\text{O.D Exposed cells})}{(\text{O.D Control cells})} \times 100 \right] \quad (1)$$

Cytotoxicity was expressed as the median lethal concentration (LC₅₀), corresponding to the concentration necessary to eliminate 50% of cells, calculated by Probit analysis using the Prism 8.0 software. The cytotoxicity was graded according to the LC₅₀ value as high cytotoxicity: LC₅₀ < 100 µg/mL, moderate cytotoxicity:

LC₅₀ > 100 to < 200 µg/mL, and potentially non-cytotoxicity: LC₅₀ > 200 µg/mL.

Antitrypanosomal activity was determined according to the percentage of infected cells and parasite amount obtained for each experimental condition by colorimetry. Parasite inhibition was calculated by equation 2, where the O.D of control corresponds to 100% of parasites. Results of antitrypanosomal activity were also expressed as EC₅₀ determined by the Probit method (Finney, 1978):

$$\% \text{ inhibition} = 1 - \left[\frac{(\text{O.D Exposed parasites})}{(\text{O.D Control parasites})} \times 100 \right] \quad (2)$$

Antiplasmodial activity of each compound was evidenced by the reduction of the O.D. The percentage of inhibition of parasitemia was calculated by Equation 2.

Antiprotozoal activity is expressed as the median effective concentration (EC₅₀) corresponding to the concentration necessary to reduce the 50% of intracellular parasites, calculated by Probit analysis using the Prism 8.0 software. The selectivity index (SI), was calculated by dividing the cytotoxic by the activity using the following formula: SI = LC₅₀ / EC₅₀.

Molecular modeling studies

Protein Structure and Setup

To explore the potential mechanism of action of hybrids **1-3,6** against two principal targets for antiparasitic drugs, the major papaine-like cysteine protease for *T. Cruzi* and *P. falciparum* were used, respectively. Thus, the crystal structure of cruzipain (PDB entry code 3IUT) and falcipain-2 in complex with E64-epoxysuccinate (PDB entry code 3BPF) were obtained from the Protein Data Bank (Ellman *et al.*, 2010; Kerr *et al.*, 2009). Discovery Studio (DS) Visualizer 2.5 was used to edit the protein structures and to remove water molecules together with bound ligands. The structures of the selected proteins were parameterized using AutoDock Tools (Morris *et al.*, 2009). In general, hydrogens were added to polar side chains to facilitate the formation of hydrogen bonds, and Gasteiger partial charges were calculated.

Ligand dataset preparation and optimization

The ligands used in this study are the **1-3** and **6** hybrids and two well-known cruzipain inhibitors: a purine nitrile and TFK (tetrafluorophenoxymethyl ketone), a very promising quinoline-based cruzipain inhibitor and epoxysuccinate (namely, E64), a potent inhibitor for FP-2. The DS visualizer was used to rewrite the data files into pdb format. The structures of the ligands were parameterized using AutodockTools to add full hydrogens to the ligands, to assign rotatable bonds, to compute Gasteiger partial atomic charges and to save the resulting structure in the required format for use with AutoDock. All possible flexible torsions of the ligand molecules were defined using AUTOTUTORS in AutoDockTools (Morris *et al.*, 1998) to facilitate the simulated binding with the receptor structure.

Docking and subsequent analysis

Docking simulations were performed with AutoDock Vina and default procedures for docking a flexible ligand to a rigid protein. Docking calculations were carried out into the binding pocket of the catalytic site of cruzipain and FP-2 structure. Once potential binding sites were identified, docking of ligands to these sites was carried out to determine the most probable and most energetically favorable binding conformations. To accomplish that, rigorous docking simulations involving a grid box to the identified binding site, Autodock Vina 1.1.2 (Trott, Olson, 2010) was used. The exhaustiveness was 20 for each protein-compound pair. The active site was surrounded by a docking grid of 38 x 38 x 38 Å with a grid spacing of 1Å. Affinity scores (in kcal/mol) given by AutoDock Vina for all ligands were obtained and ranked based on the free energy binding theory (more negative value means greater binding affinity). The resulting structures and the binding docking poses were graphically inspected to check the interactions using the DS Visualizer 2.5 (<http://3dsbiovia.com/products/>) or The PyMOL Molecular Graphics System 2.0 programs.

Ligands drug likeness evaluation

In silico drug-likeness prediction along with further ADMET (absorption, distribution, metabolism, excretion and toxicity) tools present an array of opportunities which help in accelerating the discovery of new antiparasitic drugs. To find out the drug like properties, compounds **1-3,6** were screened for their pharmacokinetic properties using opensource cheminformatics toolkits such as Molinspiration software (for MW, rotatable bonds and topographical polar surface area (PSA) descriptors), ALOGPS 2.1 algorithm from the Virtual Computational Chemistry Laboratory (for Log P_{o/w} descriptor) and the Pre-ADMET 2.0 program to predict various pharmacokinetic parameters and pharmaceutical relevant properties such as apparent intestinal permeability (App. Caco-2), binding to human serum albumin (LogK_{HSA}), MDCK cell permeation coefficients and intestinal or oral absorption (%HIA). These important parameters define absorption, permeability, motion and action of drug molecule. The interpretation of two predicted ADMET properties using the Pre-ADMET program is as follow: The value of Caco-2 permeability is classified into three classes: (1) If permeability < 4, low permeability; (2) if permeability < 70, moderate permeability; and (3) if permeability > 70, higher permeability. The value of MDCK cell permeability can be classified into three classes: (1) If permeability < 25, low permeability; (2) if 25 < permeability < 500, moderate permeability; and (3) if permeability > 500, higher permeability.

RESULTS AND DISCUSSION

Chemistry

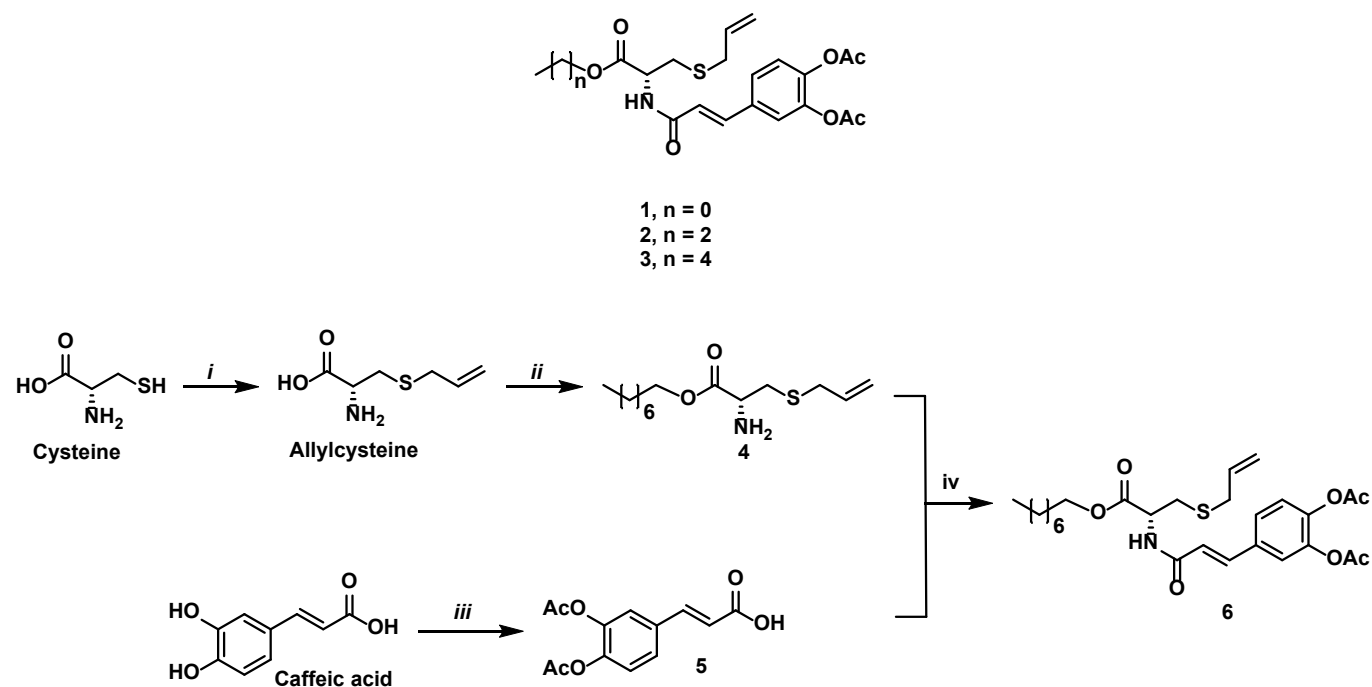
Scheme 1 shows the hybrids under study. Allyl cysteine was obtained, in 80% yield, via nucleophilic substitution between cysteine and allyl bromide. Reaction of this compound with octanol in the presence of thionyl chloride afforded the ester **4** in 60% yield. Then, compound **4** was submitted to peptide type-coupling with 3,4-diacetoxycaffeic acid **5** using HBTU as amide bond promoter, yielding hybrid **6** in 30%. In a similar way, hybrids **1-3** were obtained, these

compounds have already been reported (Castrillón *et al.*, 2019).

Biological activity

All compounds were subjected to *in vitro* evaluation of their cytotoxicity, antitrypanosomal and antiplasmodial

activity against U-937 human macrophages, intracellular amastigotes of *T. cruzi* and erythrocyte forms of *P. falciparum*, respectively. The results are summarized in tables I and II.



Reagents and conditions: (i) Allyl bromide, NH_4OH , 80% (ii) SOCl_2 , octyl alcohol, -10°C , 50%. (iii) $\text{Ac}_2\text{O}/\text{NaOH}$, caffeic acid, 80%. (iv) HBTU, Et_3N , THF, 40%.

SCHEME 1 - Synthesis of Octyl *N*-{*(2E)*-3-[3,4-bis(acetyloxy)phenyl]prop-2-enoyl}-*S*-prop-2-en-1-ylcysteinate and compounds under study.

Hybrids **1-3** were active against intracellular amastigotes of *T. cruzi* exhibiting higher activity than benznidazole. In the same way, we observed that compounds **1,2** and **6** showed activity against *P. falciparum*. Hybrids **3** and **6** were the most active over *T. cruzi* and *P. falciparum*, respectively. The anti-trypanosomal activity of compound **6** and anti-plasmodial activity of **3** were not evaluated since

the inhibition percentage at 20 $\mu\text{g}/\text{ml}$ was less than 50% (Tables I and II).

It can be seen that the activity in *T. cruzi* is dependent on the length of the alkyl chain, that is, increasing the number of carbons in odd numbers increases the activity. However, in *P. falciparum* there is no clear relationship between chain length and activity (Tables I and II).

TABLE I - *In vitro* Anti-trypanosomal activity and Cytotoxicity of S-allylcysteine ester-caffeic acid amide conjugates

Compounds	IG ^a (%) (X ± SD)	EC ₅₀ ^b (<i>T. cruzi</i> , strain Tulahuén) (µg/mL, µM)	Cytotoxicity (U-937 cells) LC ₅₀ ^d (µg/mL, µM)	SI ^e
1	54.9 ± 2.4	10.8 ± 1.0, 26.65 ± 2.37	4.8 ± 0.1, 11.4 ± 0.2	0.44
2	50.5 ± 3.8*	5.6 ± 0.8, 12.46 ± 1.78	9.4 ± 1.5, 20.9 ± 3.3	1.68
3	44.2 ± 3.3**	2.6 ± 0.1, 5.45 ± 0.21	5.1 ± 0.3, 10.7 ± 0.6	1.96
6	40.8 ± 2.3	NR ^c	10.3 ± 0.7, 19.8 ± 1.3	ND ^f
Benznidazole	60.3 ± 5.7**	10.5 ± 1.8, 40.3 ± 6.9	179.0 ± 4.2, 687.8 ± 16.1	17.0

Data represents mean value +/- standard deviation of triplicate experiments; ^aIG: Inhibition of growth; ^bEC₅₀: Effective Concentration 50; ^cNR: not performed since the % inhibition at 20 µg/ml was less than 40%. ^dLC₅₀: Lethal Concentration 50. ^eSI: Selectivity Index = LC₅₀ U-937/ EC₅₀. ^fND: it was not performed because the activity was not determined. * Concentration evaluated: 10.0 µg/mL; ** Concentration evaluated: 5.0 µg/mL;

All compounds were highly cytotoxic to U-937 cells (Table I). However, the anti-trypanosomal activity of hybrids **2** and **3** was higher than their cytotoxicity. Thus, the calculated SI (Selectivity Index) values for these hybrids were >1. As demonstrated elsewhere, benznidazole and chloroquine have moderate and very high SI values, respectively. Although hybrids **1-3**

showed better activity than benznidazole, the SI of these compounds is affected by their high cytotoxicity. These results suggest that the anti-trypanosomal activity of these compounds is selective and more active against *T. cruzi* than U-937 cells. Regarding *P. falciparum*, it is observed that all compounds were not cytotoxic against huGR cells and therefore exhibit good selectivity indices (Table II).

TABLE II - *In vitro* Anti-plasmodial and Cytotoxicity activity of S-allylcysteine ester-caffeic acid amide conjugates

Compounds	IG ^a (%) (X ± SD)	EC ₅₀ ^b (<i>P. falciparum</i> , strain 3D7) (µg/mL, µM)	Cytotoxicity (huGR cells) ^d LC ₅₀ (µg/mL, µM)	SI ^e
1	60.3 ± 8.8	13.1 ± 1.5, 31.11 ± 3.56	>200	>15.3
2	53.6 ± 7.6	12.2 ± 2.4, 27.16 ± 5.34	>200	>16.4
3	39.6 ± 7.2	NR ^c	>200	ND
6	55.9 ± 3.6	9.4 ± 0.5, 18.08 ± 0.96	>200	>21.3
Chloroquine	52.7 ± 8.3*	0.02 ± 0.01, 0.06 ± 0.03	>200	>10000

Data represents mean value +/- standard deviation of triplicate experiments; ^aIG: Inhibition of growth; ^bEC₅₀: Effective Concentration 50; ^cNR: not performed since the % inhibition at 20 µg/ml was less than 40%. ^dLC₅₀: Lethal Concentration 50. ^eSI: Selectivity Index = LC₅₀ U-937/ EC₅₀. * Concentration evaluated: 0.05 µg/mL

Computational studies

Molecular docking approach

Several protozoal proteins have been identified as druggable or potentially druggable targets, including cruzipain (TCC) and Falcipain-2 (FP-2), which are essential for virulence, infectivity and viability of insect-stage parasites (Siqueira-Neto *et al.*, 2018). In this work, we investigated the ability of conjugates of allylcysteine/caffeic acid amide to bind Cruzipain and Falcipain-2 (FP-2), the main cysteine proteases of *T. cruzi* and *P. falciparum* parasites, respectively,

and propose a plausible mechanism of action for the conjugates, selecting potential binding proteins and the most representative interactions from hybrid structures against the three-dimensional structures of selected protozoal drug-targets. Aiming at comparing ligand-binding interactions, we docked TFK and Purine nitrile as positive references for TCC, together with Epoxysuccinate (E64) and Chloroquine for FP-2 (Figure 4). It is important to notice that Chloroquine interferes with initial hemoglobin proteolysis by binding to FP-2 inducing strong conformational changes in the FP-2 structure, hence blocking the function of Falcipain-2 within the active site (Chugh *et al.*, 2013).

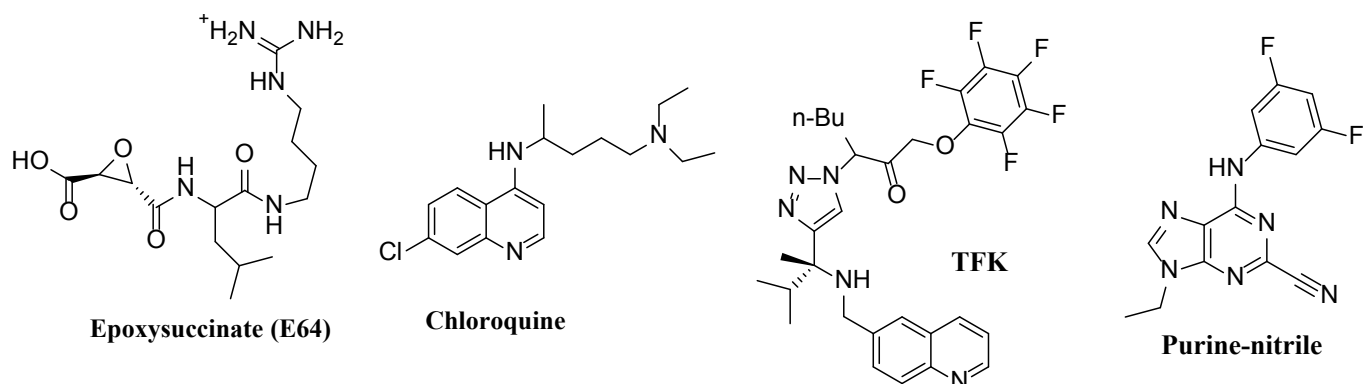


FIGURE 4 - The chemical structures of current inhibitors used as positive control in the docking studies.

Hybrids and positive references were docked inside the catalytic site of selected proteins. For this purpose, an exhaustive search in the binding pockets in order to establish key binding site points was carried out. The catalytic binding domain for TCC is characterized by the presence of 15 key amino acids residues as follows: CYS25, GLY66, GLN19, GLY23, LEU67, TRP184, GLN187, ASP161, ALA141, HIS162, GLY20, SER142, GLY163, MET145 and GLN21 (28). Hence, a grid box for TCC was set on X = 4.248, Y = 11.509 and Z = 10.261,

centering around key residues. The critical residues for the catalytic function of FP-2 involve twelve critical aminoacids: GLN36, GLY83, HIS174, CYS42, LEU172, GLY82, LEU84, TYR78, ASN173, SER149, TRP206, PHE236 (Kerr *et al.*, 2009). In this case, those key residues were enclosed in a grid box centered at X = -54.673, Y = -2.937 and Z = -16.982. Binding free energy scoring functions and ligand-interactions of conjugates and current inhibitors were calculated inside selected pockets and tabulated in Table III.

TABLE III - Best binding energy (kcal/mol) based on AutoDock scoring of the hybrids into the active sites of the protozoal drug-targets

Inhibitor	Docking score (kcal/mol)	Bonding Type	Interacting amino acids residues
TCC (PDB: 3IUT)			
1	-7.2	H-bond	GLN19, HIS162
		π - π stacked	TRP184
		π -sulfur	MET145
		π -alkyl	ALA141, HIS162
		Hydrophobic	CYS25, GLY23, GLN187, ASP161, CYS22, TRP26, GLY65, ASP140
2	-7.0	H-bond	GLN19, HIS162
		π - π stacked	TRP184
		π -sulfur	MET145
		π -alkyl	ALA141, CYS25
		Hydrophobic	GLY23, ASP161, CYS25, ALA141, GLN187, CYS22, ASN182, THR185
3	-6.8	H-bond	GLN19, HIS162
		π - π stacked	TRP184
		π -sulfur	MET145
		π -alkyl	ALA141
		Hydrophobic	GLY23, ASP161, CYS25, ALA141, GLN187, CYS22, ASN182, THR185
Purine Nitrile	-7.4	H-bond	HIS162, TRP184, GLY20
		π - π stacked	TRP184
		Halogen-F	ASP18
		Hydrophobic	GLN19, CYS22, SER24, ALA141, ASP161, CYS25, MET145, TRP188, THR185, GLN21, SER64, CYS62
TFK	-7.9	H-bond	GLN19, CYS25, GLY66
		π - π stacked	TRP184
		π -sulfur	MET145
		π - σ	SER64
		Hydrophobic	CYS22, TRP188, SER183, THR185, ASN182, TRP144, CYS63, SER64, GLY23, TRP26, ALA27, VAL139, VAL137, VAL164
FP-2 (PDB: 3BPF)			
1	-6.6	H-bond	GLN36, HIS174, GLN209
		π - π stacked	TRP206
		π -alkyl	TRP206, ALA157
		Hydrophobic	SER41, CYS39, ASN38, TRP210, ASP154, GLY207, GLY82, ALA175 SER153

TABLE III - Best binding energy (kcal/mol) based on AutoDock scoring of the hybrids into the active sites of the protozoal drug-targets

Inhibitor	Docking score (kcal/mol)	Bonding Type	Interacting amino acids residues
2	-7.2	H-bond	GLN36, HIS174, ASN173, CYS39
		π -sulfur	CYS42, LEU172
		π -alkyl	ILE85, LEU84
		Hydrophobic	ALA175, VAL150, TRP206, ASN38, LYS37, GLY40, PHE236, GLN171, VAL176, ASN86, ILE148, TRP43
6	-6.4	H-bond	GLN36, HIS174, TRP206, GLN209
		π - π stacked	TRP206
		π -alkyl	TRP206, VAL152, ALA157
		Hydrophobic	HIS174, GLN36, TRP206, VAL152, ALA157, CYS42, ASN173, SER205, ALA175, ASP35, ASN38, GLY40, CYS39
Epoxysuccinate (E64)	-6.8 (-6.7) ^a (-6.9) ^b	H-bond	GLN36, TRP206, LYS37
		Salt bridge	ASP35
		π -alkyl	ALA157, VAL152, TRP206
		Hydrophobic	HIS174, CYS42, GLY40, CYS39, SER153, GLY207, SER209, TYR106, SER205, TRP210, ASP154, SER153, SER108.
Chloroquine	-6.3 (-5.8) ^a (-6.5) ^c	π - π stacked	TRP206
		π -alkyl	ALA157, TRP210
		Hydrophobic	GLN36, CYS42, HIS174, GLN209, ASN173, GLY40, ASN38, CYS39, VAL152, SER205, PHE158, LYS37

^a according to Vijayaraghavan *et al.*, 2017; ^b according to Singh *et al.*, 2019; ^c according to Gupta *et al.*, 2011

In general, docking experiments predicted binding specific interactions between hybrids and selected protozoa targets. This computational approach revealed that hybrids based on allylcysteine-caffeic acid could block cruzipain because they displayed comparable binding affinities and interactions inside the catalytic domain (-7.2 to -6.8 kcal/mol) to those of inhibitors Purine-nitrile (-7.4 kcal/mol) and TFK (-7.9 kcal/mol). When structures were docked against FP-2 protein, good association score were obtained ranging from -6.4 to -7.2 kcal/mol in comparison with E64 and chloroquine, which had -6.6 and -6.3 kcal/mol, respectively (Table III). At this point it is worth mentioning that the docking calculations

involving these current FP-2 inhibitors afforded values in very good agreement with those reported in previous work (ranging from -5.8 to -6.9 kcal/mol) (Singh *et al.*, 2019; Vijayaraghavan, Mahajan, 2017; Gupta, Singh, Khan, 2011), hence providing confidence to the Vina scoring function of this work.

Thus, we performed a rigorous exploration of the docking solutions obtained from these compounds when docking occurred against both Cruzipain and FP-2 enzymes. Based on these different our results and upon visual inspection of 2D-ligand interaction plots, a clear behavior emerges along the molecular docking that could be summarized for each ligand-protein complex as follows:

Docking profile inside cruzipain active domain

Cruzipain has been considered the most promising target identified in *T. cruzi* for development of druggable molecules in the treatment of Chagas disease, and plays a role in the process of *Trypanosoma cruzi* adhesion and internalization into mammals, favoring the invasion of host cells and parasite replication. This proteolytic enzyme is able to digest proteins such as casein, bovine albumin and denatured hemoglobin, which strongly occurs during the course of *T. cruzi* metacyclogenesis at different stages of its life cycle (Duschak, Couto, 2009). Therefore, knocking out the development of cruzipain promotes severe alterations in the parasite metabolism affecting its maturation, host cell invasion and evasion of host defense. During efforts to characterize the role of Cruzipain in *T. cruzi*, a high-resolution crystal structure of this enzyme in the presence of TFK (as inhibitor) was solved by Ellman *et al.* (PDB: 3IUT) (Ellman *et al.*, 2010), evidencing those key amino acids in the proteolytic function of Cruzipain. This active-site cleft is located between two-domain (referred to as left (L-) and right (R-) in this work) and centered around residues CYS25, GLY66,

GLN19, GLY23, LEU67, GLY20 (R-domain), together with TRP184, GLN187, ASP161, ALA141, HIS162, SER142, GLY163 and MET145 (L-domain), which are crucial for the proteolytic activity of the TCC. In this scenario, we performed molecular docking studies to explore a possible interaction between cruzipain and hybrids **1-3**, in order to propose a mechanism of action at the molecular level. Molecular docking studies that were carried out for each of these conjugates against Cruzipain (PDB: 3IUT) within its catalytic cavity, suggest that hybrids could block the development of cruzipain. Figure 5 illustrates the most stable binding poses for active compounds **1-3** (based on AutoDock scoring listed in Table III) into the active domain of TCC. The best binding conformations for known inhibitors (purine nitrile and TFK) are also provided in order to make a valid comparison. A simple visual inspection revealed that the hybrids had docked structures that fit well within the TCC catalytic cavity, with good predicted docking scores that range from -6.8 to -7.2 kcal/mol (Table III). Superimposition of the docked inhibitors and the respective hybrids showed similar orientations, indicating that compounds **1-3** are well accommodated within the catalytic domain (Figure 5).

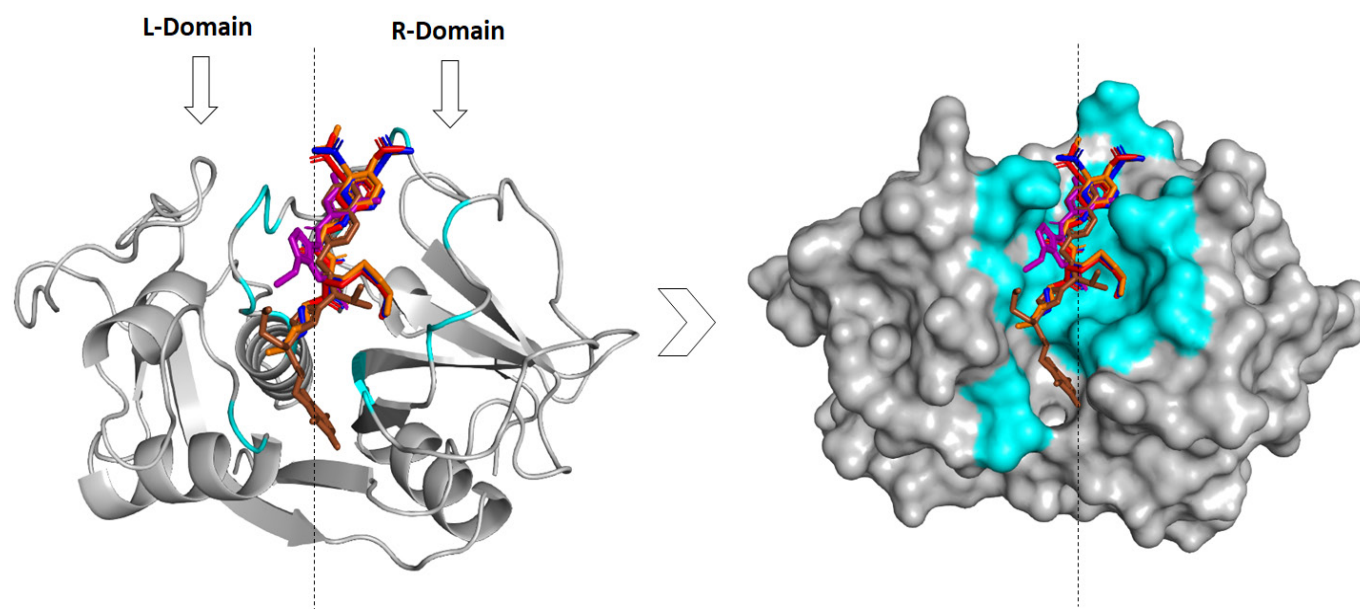


FIGURE 5 - Superposition of the best docked conformations of hybrids **1-3** and positive references within the cruzipain active site. Hybrids **1** (in red), **2** (in blue), **3** (in orange) and current inhibitors **TFK** (in brown) and **Purine-nitrile** (in purple). Critical aminoacids into cleavage site are represented in cyan.

Our docking studies revealed that hybrids **1-3** were able to bind TCC through strong non-covalent interactions, especially with those aminoacids crucial for proteolytic activity of Cruzipain (Figure 6). A notable result from our study is that the docked molecules display a fingerprint protein–ligand interaction within the active site of

Cruzipain, which includes at least nine aminoacids essential in the proteolytic function of TCC, such as CYS25, GLY66, GLN19, TRP184, GLN187, ASP161, ALA141, HIS162 and MET145. This particular result supports our hypothesis: conjugates **1-3** might block cruzipain resulting in the inhibition of *T. cruzi* intracellular.

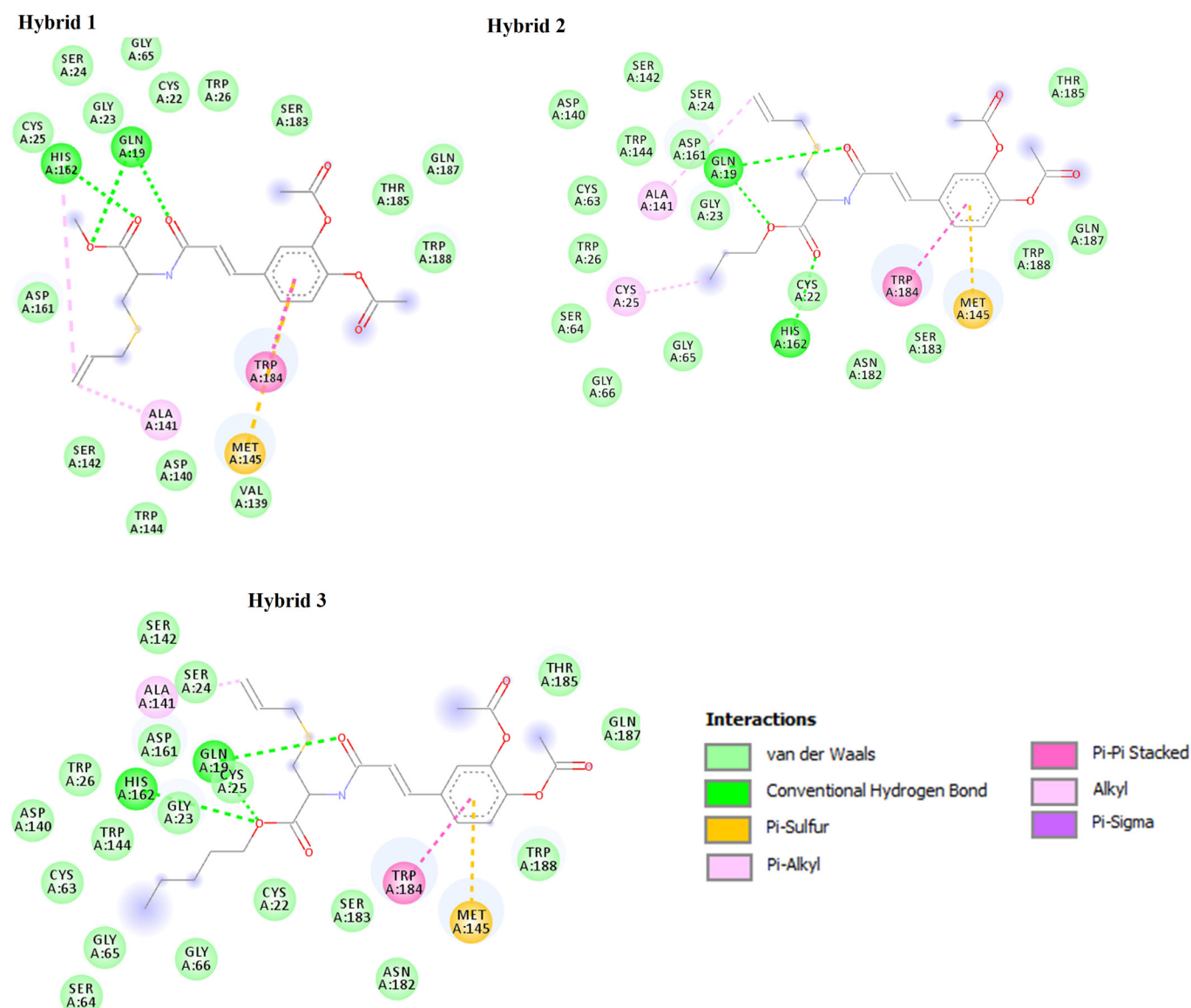


FIGURE 6 - Plotted protein-ligand interactions of hybrids **1-3** inside proteolytic pocket of Cruzipain. Dashed lines represent H-bonds and π -contacts.

An inspection of the 2D protein-ligand interaction plot after the docking procedure for hybrid **1** revealed the occurrence of three hydrogen bonds with key GLN19 and HIS162 residues, one π - π stacked contact

with Cruzipain from TRP184 and the aryl moiety of **1**, two interactions mediated through π -contacts between the allyl and aryl groups of the molecule with MET145 and ALA141 residues; several hydrophobic

contacts with CYS25, GLY23, GLN187, ASP161, CYS22, TRP26, GLY65, ASP140 residues present in the proteolytic site. Similarly, compound **2** uses three of the oxygens as hydrogen bond acceptors to key GLN19 and HIS162 aminoacids. In addition, **2** forms two critical π -contacts with TRP184 (π - π stacked) and MET145 (π -sulfur) and hydrophobic interactions with several residues postulated to bring about the catalytic function of Cruzipain (GLY23, ASP161, CYS25, ALA141, GLN187, CYS22, ASN182, THR185). As showed in Figure 6, hybrid **3** establishes very similar key interactions to those formed by **2** with Cruzipain within the proteolytic pocket.

Given the aforementioned results, we state that Cruzipain is efficiently targeted by hybrids **1-3** probably through non-covalent interactions with those critical residues crucial for TCC proteolytic activity. Therefore, the marked activity found during *in vitro* assays may be explained considering cruzipain inhibition as plausible mechanism for killing *T. cruzi*. Thus, we strongly suggest that the allyl cysteine-caffeic acid combination represents a novel Cruzipain binding motif that can be exploited for further anti-trypanosomal drug design with moderate potency. Although more experimental assays should be further explored in order to validate the predicted observations.

Docking profile within FP-2 hemoglobin cleavage site

Falcpain-2 (FP-2) is the most important papain-like cysteine protease in *P. falciparum* and plays a crucial role both in the parasite life cycle and in parasite virulence by degrading erythrocyte proteins, most notably host hemoglobin. Designing inhibitors capable of blocking hemoglobin hydrolysis on FP-2 prevents parasite development, and therefore constitutes a promising starting point to develop new antimalarial drugs. It has now been well established that the hemoglobin cleavage site on FP-2 contains residues important for protein function including GLN36, GLY83, HIS174, CYS42, LEU172, GLY82, LEU84, TYR78, ASN173, SER149, TRP206 and PHE236. Our computational investigations revealed that hybrids **1,2,6** could block the hemoglobin cleavage cavity of Falcpain-2 interfering with parasite maturation. Thus, a possible disruption of FP-2 function by hybrids **1,2,6** was suggested by the docking results, which based on the most stable conformations obtained by AutoDock (Table III), it showed that hybrids **1,2,6** can accommodate themselves into energetically favorable poses along the catalytic domain of FP-2. The superposition of the positive references (E64 and chloroquine) and the best conformation obtained theoretically for selected docked compounds shows how these hybrids are capable of occupying the catalytic pocket during the docking process (Figure 7).

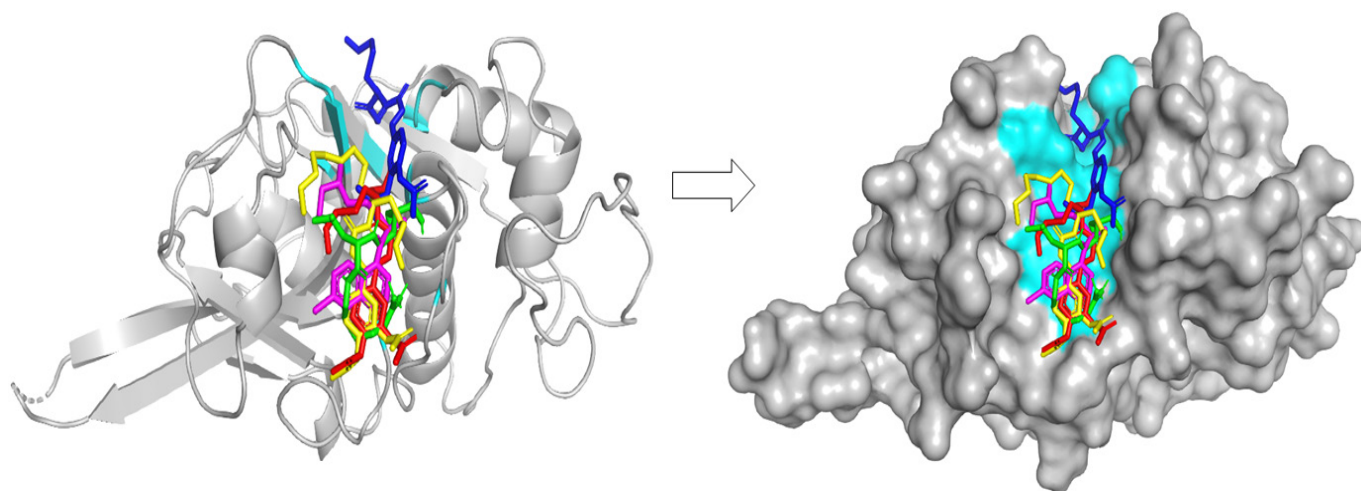


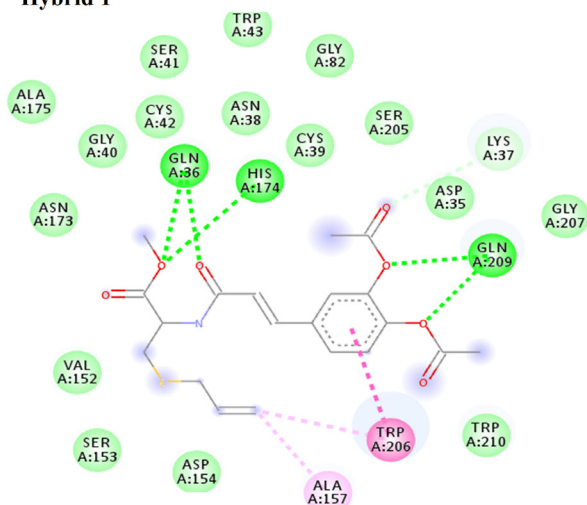
FIGURE 7 - Superposition of the best docked conformation of hybrids **1,2,6** and positive references alongside the hemoglobin cleavage site on FP-2. Hybrids **1** (in red), **2** (in blue), **6** (in yellow) and current inhibitors **E64** (in green) and **Chloroquine** (in magenta). Critical aminoacids into the hemoglobin cleavage site are represented in cyan.

It is interesting to see that all hybrids had at least four interactions with those residues in FP-2 crucial to parasite survival, through H-bonds, π -contacts or hydrophobic contacts, making them a promising scaffold that may be used against the malaria infection. As such, in searching for those critical contacts that could block the catalytic site in Falcipain-2, an exhaustive analysis of the docking results for conjugates was carried out as discussed below.

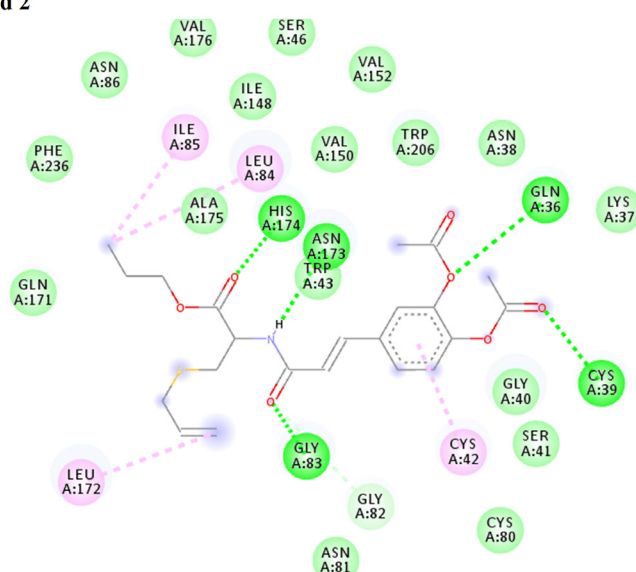
As shown in Figure 8, the active molecules complexed to the FP-2 protein had an interaction fingerprint involving seven critical residues involved in the Falcipain-2 cleavage function: GLN36, HIS174, GLU83, CYS42, LEU172, TRP206 and ASN173. Thus, hybrid **1** displayed two strong H-bonds through binding between ester and amide moieties and key GLN36 and HIS174 residues, respectively. Critical residue TRP206 from FP-2 was also involved in the interaction by forming one π - π stacked contact with **1**, while CYS42 and ASN173 residues were found to be involved in the binding through van der Waals contacts. In addition to those crucial aminoacids, several interactions of **1** with the FP-2 protein in the cleavage site were observed as follows: one hydrogen bond between both acetyl groups

and GLN209, one π alkyl contact with ALA157 and allyl moiety of **1**, and various hydrophobic interactions with SER41, CYS39, ASN38, TRP210, ASP154, GLY207, GLY82, ALA175 and SER153 that would play a crucial role in the stabilization of the ligand during the binding event. Protein-ligand interaction analysis of hybrid **2** (which had the best docking score of $-7.2 \text{ kcal}\cdot\text{mol}^{-1}$) to the FP-2 revealed that this molecule binds firmly within the target site of FP-2 through three conventional hydrogen bonds with critical GLN36, GLY83, HIS174, ASN173 residues, and four π -alkyl interactions with the crucial residues ILE85, LEU172, CYS42 and ILE85. Additionally, numerous van der Waals contacts formed between hybrid **2** and ALA175, VAL150, TRP206, ASN38, LYS37, GLY40, PHE236, GLN171, VAL176, ASN86, ILE148 and TRP43 aminoacids were also observed, these contacts may have important roles in stabilizing the binding event. Similarly, hydrogen bonds, π - π stacking and hydrophobic interactions were observed in the docking results between hybrid **6** and key residues for FP-2 cleavage function, including HIS174, GLN36, TRP206, VAL152, ALA157, CYS42, ASN173, SER205, ALA175, ASP35, ASN38, GLY40, CYS39, respectively.

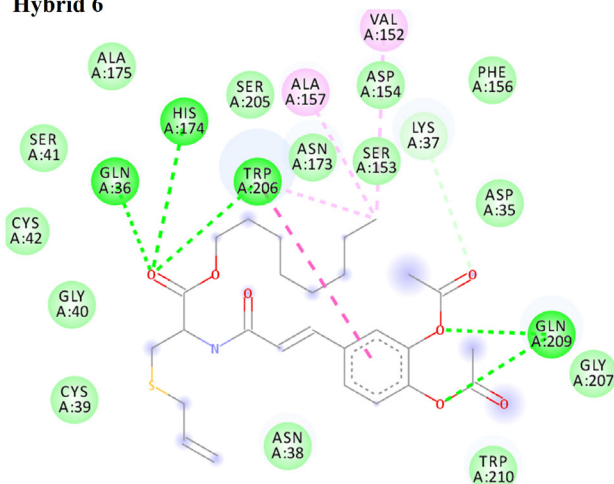
Hybrid 1



Hybrid 2



Hybrid 6



Interactions

	van der Waals		Pi-Pi Stacked
	Conventional Hydrogen Bond		Alkyl
	Carbon Hydrogen Bond		Pi-Alkyl

FIGURE 8 - 2D interaction modes plots for hybrids **1,2,6** inside hemoglobin cleavage site on FP-2. Interactions between each component and residues of FP-2 are indicated by the dashed lines

In accordance with the docking results, allylcysteine–caffeic acid hybrids display strong preference for the hemoglobin cleavage site on FP-2. The consequence would be, that the hybrids are capable to block *P. falciparum* development by FP-2 disrupting. Hence, we suggest that conjugates have antimalarial activity by the possible mechanism of FP-2 inhibition, making them a new scaffold to develop novel antimalarial agents by targeting Falcipain-2.

In addition, the results of our docking investigations of the biologically active compounds clearly revealed

that more favorable contributions of van der Waals interactions were attached when the length of the alkyl chain increased, hence hybrids could create more interactions between the alkyl chain with those hydrophobic residues in the selected protozoa targets, leading to much more effective molecular recognition. This finding highlighted the importance of hydrophobic interactions in the stabilization of the ligands during the binding event.

Pharmacokinetic properties and in silico ADME studies

Calculated drug-likeness profiles play a critical role in assessing the quality of novel anti-parasitic candidates. Early predictions of pharmacokinetic behaviour of the promising anti-protozoal compounds based on their

structures could help find safer and more effective leads for preclinical testing. In this paper, we calculated the most important pharmacokinetic and ADME indices for conjugates **1-3** and **6** in order to examine their drug-like potentials (Table IV). Our results revealed the druggability of the hybrids, demonstrating their potential as likely orally active antiparasitic candidates.

TABLE IV - *In silico* pharmacokinetic and ADME indices of conjugates **1-3,6**

Entry	M.W ^a	PSA ^b	n-Rot Bond (0-10)	n-ON ^c	n-OHNH ^d	Log P _{o/w} ^e	Log K _{HSA} ^f	App. Caco-2 ^g	App. MDCK (nm/s) ^h	% HIA ⁱ	Lipinski Rule of five (≤1)
Caffeic acid	180.160	96.196	2.0	4.0	3.0	0.538	-0.803	21	10	75.8	0
Allylcysteine	161.218	72.680	5.0	3.0	3.0	-1.533	-0.891	23	17	83.9	0
1	421.464	129.800	11.0	8.0	1.0	3.025	-0.236	530	321	64.2	1
2	449.518	123.439	13.0	8.0	1.0	3.960	-0.029	1011	754	66.4	1
3	477.571	129.308	15.0	8.0	1.0	4.686	0.284	621	389	64.4	1
6	519.652	129.377	18.0	8.0	1.0	5.597	0.527	834	513	86.0	1

[a] Molecular weight of the hybrid (150-500). [b] Polar surface area (PSA) (7.0–200 Å²). [c] n-ON number of hydrogen bond acceptors <10. [d] n-OHNH number of hydrogens bonds donors ≤5. [e] Octanol/water partition coefficient (LogP_{o/w}) (-2.0 to 6.0). [f] Binding-serum albumin (K_{HSA}) (-1.5 to 1.5). [g] Human intestinal permeation (<25 poor, >500 great). [h] Madin-Darby canine kidney (MDCK) cells permeation. [i] Human intestinal absorption (% HIA) (>80% is high, <25% is poor).

Interestingly, favorable pharmacokinetics indices were found for our conjugates compared to 95% of approved drugs. According to Lipinski's rule of five (no more than one violation is acceptable) (Lipinski *et al.*, 1997) the tested compounds could be used as orally dosed drugs in humans. All the hybrids had ideal human intestinal absorption (% HIA) numbers ranging from 64.2 to 86%, this suggests that the hybrids could be absorbed throughout the intestinal segments upon oral administration. Despite that high degrees of lipophilicity (calculated as LogP_{o/w}) were found for all the compounds (3.025 - 5.597), they all fit well within the optimal range for lipid-based formulations (-2.0 to 6.0) (Ditzinger *et al.*, 2019).

Polar Surface Area (PSA) is the most important physicochemical property to correlate passive molecular transport through membranes and drug-membrane interactions. Predicted PSA values for hybrids **1-3,6** showed acceptable therapeutic values (ranging from

123.439 to 129.377 Å²), indicating that these smaller compounds would penetrate more efficiently through the infected host cells. Moreover, in silico passive transmembrane permeation was calculated for all hybrids using Caco-2 cell monolayers or MDCK cells as model. Currently, both models are recommended as a simplified in vitro model of intestinal absorption in drug development. It was found that the four conjugates display good permeability values (ranging from 321 to 1011 nm/s). Finally, we investigated the ability of the hybrids to bind to serum albumin (expressed as logK_{HSA}), which is the most significant parameter for distribution and transport of anti-parasitic drugs in the systemic circulation. For therapeutic uses, LogK_{HSA} values in the range of -1.5 to 1.5 are recommended for potential drugs. Notably, all hybrids fit well within the recommended values showing LogK_{HSA} numbers between -0.236 to 0.527. According to the above-mentioned results, merging allylcysteine

and caffeic acid sub-units to a unique structural core provides active compounds with optimal pharmacokinetic properties, making this scaffold promissory to develop candidates to fight against protozoal diseases.

Bioavailability radar plot for conjugates 1-3,6

A further consideration in the use of hybrids **1-3** and **6** as potential oral antiparasitic agents was visually inspected by using bioavailability radar diagrams, a procedure that is both time- and cost-effective to visually display behavior as oral drugs. The radar chart provided a valuable tool to determine if the test molecules fall within the optimal ranges for 95% of current drugs. Here, we investigated six important drug-likeness properties by using a multi-color radar plotted for hybrids **1-3** and **6**. As illustrated in Figure 9, molecular weight (MW), number of rotatable bonds, PSA, $\text{LogP}_{o/w}$, H-bonds acceptors n-ON and donors n-OHNH are presented on the axes of

a hexagonal radar plot (yellow area) and compared with the optimal range for 95% of the marketed oral drugs (gray area).

A visual inspection of bioavailability radar plots for conjugates **1-3** and **6**, revealed that the calculated pharmacokinetic parameters are in accordance with a typical radar plot for an oral drug-like molecule. As illustrated in figure 9, MW, PSA, $\text{LogP}_{o/w}$, H-donor, H-acceptor properties are within the optimal range for 95% of the FDA-approved drugs. However, radar plots showed one violation exceeding the number of free rotating bonds (less than or equal to 10) for all hybrids evaluated (displaying more than 11), due to numerous flexible alkyl chains present in the structure. However, this finding is currently acceptable for an orally active drug and does not pose a problem as demonstrated recently, which n-Rot Bond descriptor presents less influence on bioavailability requirement in comparison with PSA descriptor.

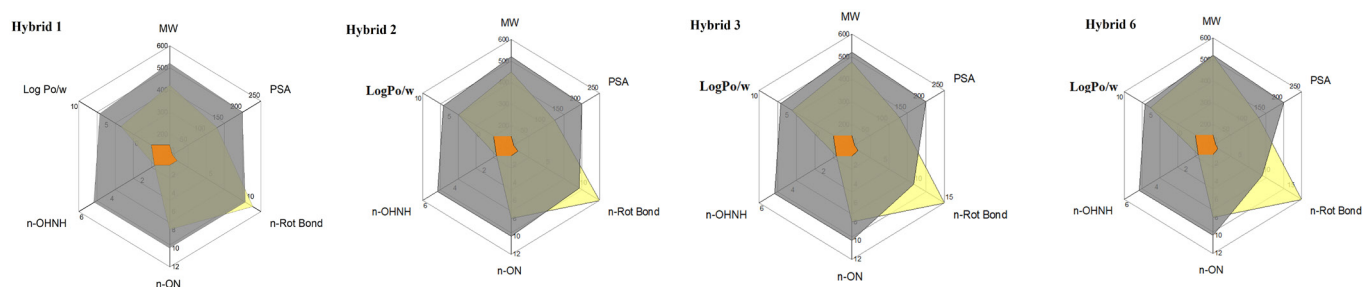


FIGURE 9 - The bioavailability radar plots of the active hybrids **1-3,6**: the gray area represents the optimal range for 95% of the FDA-approved drugs. The yellow area represents calculated drug-likeness properties of hybrids. The orange zone indicating low oral bioavailability.

In vitro Assessment of Metabolic Stability

Evaluation of metabolic stability of a potential drug-candidate is one of the biggest challenges in pharmaceutical research. Early *in vitro* testing and prediction of metabolic stability plays an important role in drug development, providing valuable information for discovery teams about oral bioavailability, intrinsic clearance and the formation of toxic metabolites of potential prospects. However, *in vitro* metabolic stability testing often requires automated, laborious

manual manipulations and robust assays. Nowadays, computer-aided tools provide a rapid metabolic stability screening of large compound sets at a lower cost. In this scenario, MetStabOn is a powerful online server for the qualitative prediction of metabolic stability (expressed as $T_{1/2}$, low (≤ 0.6 h), medium (0.6 - 2.32 h) or high (>2.32 h)) which is based on *in vitro* assays performed on liver microsomes referring to human, rat and mouse experiments (Podlewska, Kafel, 2018). In this work, MetStabOn was used to calculate the metabolic stability for hybrids **1-3,6** in order to get a broader insight into

the first-pass metabolism and bioavailability. As can be seen in Table V, metabolic stability data obtained for human, rat, and mouse models showed that hybrids **1-3,6** display half-lifetimes values belonging to medium (0.6 - 2.32 h) and high (>2.32 h) stability class. Particularly, data referring to human model displays half-lifetime values higher than 0.6 h, leading to molecules belonging to the group of medium metabolic stability. Notably, hybrids **1-3,6** had a high metabolic stability (>2.32 h) when liver microsomes of rat model was used. Finally, satisfactory results were found for the metabolic stability of hybrids based on mouse models exhibiting medium values (ranging from 0.883 to 0.997 h) of half-lifetimes. Thus, metabolic stability examinations based on different species revealed that active hybrids **1-3,6** would have low hepatic first-pass metabolism and sufficient time to produce the desired therapeutic response.

TABLE V - Predicted metabolic stabilities for hybrids 1-3,6

ybrid	$T_{1/2}$ [hr] ^{a,b}		
	Human	Rat	Mouse
1	0.786	7.586	0.997
2	0.690	3.93	0.972
3	0.665	4.808	0.883
6	0.663	3.824	0.991

^a Estimated metabolic stability produced on liver microsomes; ^b Metabolic stability cutoffs as follows ($T_{1/2}$ expressed in hours): ≤ 0.6 (Low), 0.6 - 2.32 (Medium) and >2.32 (High).

According to the *in-silico* predictions, merging allylcysteine and caffeic acid sub-units to unique structural core provide active compounds with optimal biopharmaceutical indices, making this scaffold promissory to develop oral candidates to fight protozoal diseases.

In summary, this paper showed the identification of promising antiprotozoal candidates based on biological studies and molecular modeling. By integrating *in silico* approaches, we evidenced that hybrids **1-3,6** could act by disrupting normal functions of Cruzipain (in the Chagas case) and Falcipain-2 (in the malaria

case). Docking experiments predicted binding poses and critical interactions with these proteins. These interesting findings suggest a possible inhibition of both enzymes as molecular mechanism for hybrids, which could explain the marked *in vitro* anti-protozoal activity obtained for these compounds. Finally, we identified that *S*-allylcysteine ester-caffeic acid amide conjugates bears optimal pharmacokinetics properties to be used orally as a potential antiparasitic option. Therefore, we suggest that these compounds should be taken into consideration as scaffold for drug development against protozoal diseases.

CONCLUSIONS

The synthesis and characterization of one new class of hybrids based on *S*-allylCysteine Ester/Caffeic Acid Amide is reported in this work. The antiprotozoal activity of this compound and of other three hybrids was evaluated. Our results show that hybrid **6** was the most active against *T. cruzi*, whereas compound **3** was the most active over *P. falciparum*. None of the hybrids were cytotoxic against huGR cell line. The SAR analysis showed that the anti-trypanosomal activity is directly related to increasing the length of the alkyl chain by an odd number of carbon atoms. However, in *P. falciparum* there is no clear relationship between chain length and activity. In addition, in order to propose a molecular explanation for understanding the anti-protozoal activity of the hybrids, we performed molecular modeling studies based on binding modes and protein–ligand interactions with critical enzymes for the development of Chagas and Malaria infections. It was observed that the hybrids had a good predicted binding affinity to the protozoa related enzymes (particularly, Cruzipain and Falcipain-2) as compared to current inhibitors. The studied hybrids firmly bind to these targets through several interactions with those key residues involved in the catalytic mechanisms. This work shows strong evidence that hybrid **6** could act as anti-protozoal candidate by Cruzipain (for Chagas disease) inhibition, while compound **3** may act against FP-2 (for Malaria infection). Moreover, conjugates **1-3** and **6** present optimal ADME characteristics, making them a potentially safe alternative to orally treat a protozoal infection. In summary, hybrid compounds based on

allylcysteine and caffeic acid could be a novel scaffold to develop promising candidates for future anti-protozoal studies. However, further studies will have to address the stability of protein-ligand complexes by molecular dynamics simulations and enzymatic assays will also have to be carried out to support the interaction of hybrids with targets predicted in this work.

ACKNOWLEDGMENTS

The authors thank COLCIENCIAS (Grant No. 247-2016, code: 111571249830), CIDEPRO and Universidad de Antioquia for financial support. The authors wish to thank Dr. Sabina Podlowska for their work in estimated metabolic stability (Institute of Pharmacology, Polish Academy of Sciences, Department of Medicinal Chemistry)

CONFLICT OF INTEREST

The authors declare no conflict of interest.

REFERENCES

- Alson SG, Jansen O, Cieckiewicz E, Rakotoarimanana H, Rafatro H, Degotte G, et al. In-vitro and in-vivo antimalarial activity of caffeic acid and some of its derivatives. *J Pharm Pharmacol*. 2018;70(10):1349-1356.
- Borchhardt DM, Mascarello A, Chiaradia, LD. Nunes RJ. Oliva G. Yunes RA, et al. Biochemical evaluation of a series of synthetic chalcone and hydrazide derivatives as novel inhibitors of cruzain from *Trypanosoma cruzi*. *J Braz Chem Soc*. 2010;21(1):142–150.
- Castrillón W, Herrera-R A, Prieto LJ, Conesa-Milián L, Carda M, Naranjo T, et al. Synthesis and in vitro evaluation of S-allyl cysteine ester - caffeic acid amide hybrids as potential anticancer agents. *Iran J Pharm Res*. 2019;18(4):1770-1789.
- Chatelain E, Ioset JR. Drug discovery and development for neglected diseases: the DNDi model. *Drug Des Devel Ther*. 2011;5:175-181.
- Chugh, M, Sundararaman V, Kumar S, Reddy VS, Siddiqui WA, Stuart K, et al. P. Protein complex directs hemoglobin-to-hemozoin formation in *Plasmodium falciparum*. *Proc Natl Acad Sci USA*. 2013;110(14):5392-5397.
- Coa JC, Yepes A, Carda M, Conesa-Milián L, Upegui Y, Robledo SM, et al. Synthesis, In silico studies, antiprotozoal and cytotoxic activities of quinoline-biphenyl hybrids. *ChemistrySelect*. 2020;5(10):2918-2924.
- Coppi A, Cabinian M, Mirelman D, Sinnis P. Antimalarial activity of allicin, a biologically active compound from garlic cloves. *Antimicrob Agents Chemother*. 2006;50(5):1731-1737.
- De P, Bedos-Belval F, Vanucci-Bacquéa C, Baltas M. Cinnamic acid derivatives in tuberculosis, malaria and cardiovascular diseases - a review. *Curr Org Chem*. 2012;16(6):747-768.
- Ditzinger F, Price DJ, Ilie AR, Köhl NJ, Jankovic S, Tsakiridou G, et al. Lipophilicity and hydrophobicity considerations in bio-enabling oral formulations approaches - a PEARL review. *J Pharm Pharmacol*. 2019;71(4):464-482.
- Duschak V, Couto A. Cruzipain, the major cysteine protease of *trypanosoma cruzi*: a sulfated glycoprotein antigen as relevant candidate for vaccine development and drug target. A review. *Curr Med Chem*. 2009;16(24):3174-202.
- Duschak VG, Ciaccio M, Nassert JR, Basombrio MA. Enzymatic activity, protein expression, and gene sequence of cruzipain in virulent and attenuated *Trypanosoma cruzi* strains. *J Parasitol* 2001;87(5):1016-1022.
- Ellman J, Brak K, Kerr D, Barrett K, Fuchi N, Debnath M. et al. Nonpeptidic tetrafluorophenoxymethyl ketone cruzain inhibitors as promising new leads for chagas disease chemotherapy. *J Med Chem*. 2010;53(4):1763-1773.
- Fidock DA, Rosenthal PJ, Croft SL, Brun R, Nwaka S. Antimalarial drug discovery: Efficacy models for compound screening. *Nat Rev Drug Discov*. 2004;3(6):509-520.
- Fujii N, Mallari JP, Hansell EJ, Mackey Z, Doyle P, Zhou YM, et al. Discovery of potent thiosemicarbazone inhibitors of rhodesain and cruzain. *Bioorg Med Chem Lett*. 2005;15(1):121-123.
- Finney JD. Probit Analysis: Statistical Treatment of the Sigmoid Response Curve, 3rd ed.; Cambridge University Press: Cambridge, UK, 1978. p. 550.
- Foroutan-Rad M, Hazrati TK, Khademvatan S. Antileishmanial and Immunomodulatory Activity of *Allium sativum* (Garlic): A Review. *J Evid Based Complementary Altern Med*. 2017;22(1):141-155.
- García E, Ochoa R, Vásquez I, Conesa-Milián L, Carda M, Yepes A, et al. Furanchalcone–biphenyl hybrids: synthesis, in silico studies, antitrypanosomal and cytotoxic activities. *Med Chem Res*. 2019;28:608–622.
- Gupta A, Saha P, Descôteaux C, Leblanc V, Asselin E, Bérubé G. Design, synthesis and biological evaluation of estradiol-chlorambucil hybrids as anticancer agents. *Bioorg Med Chem Lett*. 2010;20(5):1614-1618.

- Gupta Ch, Singh S, Khan A. Molecular docking studies of antimalarial drug and its analogues against falcipain-2 protein. *Inter J Biosol.* 2011;1:16-21.
- Hans-Hartwig O, Tanja S. Cysteine proteases and their inhibitors. *Chem Rev.* 1997;97(1):133–172.
- Hung CC, Tsai WJ, Kuo LM, Kuo YH. Evaluation of caffeic acid amide analogues as anti-platelet aggregation and anti-oxidative agents. *Bioorg Med Chem.* 2005;13(5):1791-1797.
- Ivasiv V, Albertini C, Gonçalves AE, Rossi M, Bolognesi ML. Molecular hybridization as a tool for designing multitarget drug candidates for complex diseases. *Curr Top Med Chem.* 2019;19(19):1694-1711.
- Keenan M, Chaplin JH. A new era for chagas disease drug discovery? *Prog Med Chem.* 2015;54:185-230.
- Kerr ID, Lee JH, Pandey K, Harrison A, Sajid M, Rosenthal PJ, et al. Structures of falcipain-2 and falcipain-3 bound to small molecule inhibitors: implications for substrate specificity. *J Med Chem.* 2009;52(3):852-857.
- Kunakbaeva Z, Carrasco R, Rozas I. An approximation to the mechanism of inhibition of cysteine proteases: nucleophilic sulphur addition to Michael acceptors type compounds. *J Mol Struc-THEOCHEM.* 2003;626(1):209-216.
- Lipinski CA, Lombardo F, Dominy BW, Feeney PJ. Experimental and computational approaches to estimate solubility and permeability in drug discovery and development settings. *Adv Drug Deliv Rev.* 1997;23(1-3):3-25.
- Londoño F, Cardona W, Alzate F, Cardona F, Vélez ID, Upegui Y, et al. Antiprotozoal activity and cytotoxicity of extracts from *Solanum arboreum* and *S. ovalifolium* (Solanaceae). *J Med Plants Res.* 2016;10(8):100-107.
- Machin JM, Kantsadi AL, Vakonakis I. The complex of *Plasmodium falciparum* falcipain-2 protease with an (E)-chalcone-based inhibitor highlights a novel, small, molecule-binding site. *Malar J.* 2019;18:388-401.
- Meunier B. Hybrid molecules with a dual mode of action: dream or reality? *Acc Chem Res.* 2008;41(1):69–77.
- Morris GM, Goodshell DS, Halliday RS, Huey R, Hart WE, Belew RK, et al. Docking using a Lamarckian genetic algorithm and empirical binding free energy function. *J Comput Chem.* 1998;19(14):1639-1662.
- Morris GM, Huey R, Lindstrom W, Sanner MF, Belew RK, Goodsell DS, et al. AutoDock4 and AutoDockTools4: Automated docking with selective receptor flexibility. *J Comput Chem.* 2009;30(16):2785-2791.
- McGrath ME, Eakin AE, Engel JC, McKerrow JH, Craik CS, Fletterick RJ. The crystal structure of cruzain: a therapeutic target for Chagas' disease. *J Mol Biol.* 1995;247(2):251-259.
- McKerrow JH, Caffrey C, Kelly B, Loke P, Sajid M. Proteases in parasitic diseases. *Annu Rev Pathol.* 2006;1:497-536.
- Nkhoma S, Molyneux M, Ward S. In vitro antimalarial susceptibility profile and *prcr*/*pfmdr-1* genotypes of *Plasmodium falciparum* field isolates from Malawi. *Am J Trop Med Hyg.* 2007;76(6):1107-1112.
- Nok AJ, Williams S, Onyenekwe PC. Allium sativum-induced death of African trypanosomes. *Parasitol Res.* 1996;82(7):634-637.
- Otero E, García E, Palacios G, Yepes LM, Carda M, Agut R, et al. SM. Triclosan-caffeic acid hybrids: Synthesis, leishmanicidal, trypanocidal and cytotoxic activities. *Eur J Med Chem.* 2017;141:73-83.
- Otero E, Robledo S, Díaz S, Carda M, Muñoz D, Paños J, et al. Synthesis and leishmanicidal activity of cinnamic acid esters: structure–activity relationship. *Med Chem Res.* 2014;23:1378-1386.
- Podlewska S, Kafel R. MetStabOn-Online platform for metabolic stability predictions. *Int J Mol Sci.* 2018;19(4):1040-1056.
- Provencher-Mandeville J, Descôteaux C, Mandal SK, Leblanc V, Asselin E, Bérubé G. Synthesis of 17beta-estradiol-platinum(II) hybrid molecules showing cytotoxic activity on breast cancer cell lines. *Bioor Med Chem Lett.* 2008;18(7):2282–2287.
- Rajan P, Vedernikova I, Cos P, Berghe DV, Augustyns K, Haemers A. Synthesis and evaluation of caffeic acid amides as antioxidants. *Bioorg Med Chem Lett.* 2001;11(2):215-257.
- Santos MM, Moreira R. Michael acceptors as cysteine protease inhibitors. *Mini Rev Med Chem.* 2007;7(10):1040-1050.
- Shapiro A, Nathan HC, Hutner SH, Garofalo J, McLaughlin SD, Rescigno D, et al. In Vivo and In Vitro Activity by Diverse Chelators against *Trypanosoma brucei brucei*. *J Protozool.* 1982;29(1):85-90.
- Siles R, Chen SE, Zhou M, Pinney KG, Trawick ML. Design, synthesis, and biochemical evaluation of novel cruzain inhibitors with potential application in the treatment of Chagas' disease. *Bioorg Med Chem Lett.* 2006;16(16):4405-4409.
- Singh A, Kalamuddin M, Mohammed A, Malhotra P, Hoda N. Quinoline-triazole hybrids inhibit falcipain-2 and arrest the development of *Plasmodium falciparum* at the trophozoite stage. *RSC Adv.* 2019;9(67):39410-39422.
- Siqueira-Neto JL, Debnath A, McCall LI, Bernatchez JA, Ndao M, Reed SL, et al. Cysteine proteases in protozoan parasites. *PLoS Negl Trop Dis.* 2018;12(8):6512-6524.
- Son S, Lewis BA. Free radical scavenging and antioxidative activity of caffeic acid amide and ester analogues:

structure-activity relationship. *J Agric Food Chem.* 2002;50(3):468-472.

Tasdemir D, Kaiser M, Brun R, Yardley V, Schmidt TJ, Tosun F, et al. Antitrypanosomal and antileishmanial activities of flavonoids and their analogues: in vitro, in vivo, structure-activity relationship, and quantitative structure-activity relationship studies. *Antimicrob Agents Chemother.* 2006;50(4):1352-1364.

Tiwari HK, Kumar P, Kumar K, Jatana N, Garg S, Narayanan L, et al. In vitro antimalarial evaluation of piperidine- and piperazine-based chalcones: inhibition of falcipain-2 and plasmepsin II hemoglobinases activities from *Plasmodium falciparum*. *ChemistrySelect.* 2017;2(25):7684-7690.

Trott O, Olson AJ. AutoDock Vina: improving the speed and accuracy of docking with a new scoring function, efficient optimization and multithreading. *J Comput Chem.* 2010;31(2):455-461.

Tsogoeva SB. Recent progress in the development of synthetic hybrids of natural or unnatural bioactive compounds for medicinal chemistry. *Mini Rev Med Chem.* 2010;10(9):773-793.

Viegas-Junior C, Danuello A, Bolzani VD, Barreiro E, Fraga C. Molecular hybridization: a useful tool in the design of new drug prototypes. *Curr Med Chem.* 2007;14(17):1829-1852.

Vieira RP, Santos VC, Ferreira RS. Structure-based Approaches Targeting Parasite Cysteine Proteases. *Curr Med Chem.* 2019;26(23):4435-4453.

Vijayaraghavan Sh, Mahajan S. Docking, synthesis and antimalarial activity of novel 4-anilinoquinoline derivatives. *Bioorg Med Chem Lett.* 2017;27(8):1693-1697.

World Health Organization (WHO). Neglected tropical diseases. 2018a. Available online: http://www.who.int/neglected_diseases/diseases/en/ (accessed on 20 June 2020)

World Health Organization (WHO). World Malaria Report 2018. 2018b. Available online: <https://www.who.int/malaria/publications/world-malaria-report-2018/report/en/> (accessed on 04 March 2020).

World Health Organization (WHO) Chagas disease (American Trypanosomiasis). 2019. [http://www.who.int/news-room/fact-sheets/detail/chagasdisease-\(american-trypanosomiasis\)](http://www.who.int/news-room/fact-sheets/detail/chagasdisease-(american-trypanosomiasis)). (Accessed 04 March 2020).

Yang Z, Fonović M, Verhelst SH, Blum G, Bogyo M. Evaluation of alpha,beta-unsaturated ketone-based probes for papain-family cysteine proteases. *Bioorg Med Chem.* 2009;17(3):1071-1078.

Received for publication on 31st August 2020

Accepted for publication on 05th April 2021